Respiratory Research

RESEARCH

Open Access

Multiomic and functional validation of ACSL3, a regulator of fatty acid metabolism, as a lymph node metastasis-associated gene in lung adenocarcinoma

Yicheng Liang[1,2†], Linchuan Liang[2†], Minjun Du[2†], Yangyang Lei[3†], Yushun Gao[2*] and Shanqing Li[1*]

Abstract

Background This study investigates the role of fatty acid metabolism (FAM)-related genes in lymph node metastasis (LNM) and prognosis of lung adenocarcinoma (LUAD) and elucidates the underlying mechanisms.

Methods Transcriptomic and single-cell RNA-seq data from TCGA and GEO were integrated to identify FAM-related genes. Non-negative matrix factorization clustering and univariate Cox regression were applied to develop a FAM-based prognostic risk model (FScore). Associations of FScore with gene mutations and tumor microenvironment features were analyzed. Immunohistochemistry, and functional assays were performed to alidate the role of ACSL3 in LUAD malignancy and lymphangiogenesis.

Results A five-gene FAM-related risk signature (ACSL3, MCAT, NDUFAB1, OLAH, ACSL4) was identified. The derived FScore stratified patient prognosis across multiple independent cohorts, with high FScore linked to significantly worse overall survival. FScore increased progressively with nodal stage (N0 < N1 < N2) and correlated with an immunosuppressive "cold" tumor microenvironment and specific mutation patterns (e.g., low FLG mutation). Single-cell and spatial transcriptomics revealed cell-type–specific FAM activity, predominantly in epithelial, mast, and myeloid cells. ACSL3 was overexpressed in LUAD tissues and served as an independent poor prognostic factor. ACSL3 overexpression elevated intracellular triglyceride and phospholipid levels, upregulated key FAM enzymes (FASN, ACC, ACLY) and the c-Myc/VEGFC axis, promoted proliferation, migration, invasion, and lymphangiogenesis, while suppressing apoptosis.

Conclusions The FScore serves as a robust predictor of LNM and poor prognosis in LUAD. ACSL3 drives lymphatic metastasis via the c-Myc/VEGFC axis, positioning ACSL3 as a potential therapeutic target to suppress LNM in LUAD.

†Yicheng Liang, Linchuan Liang, Minjun Du and Yangyang Lei contributed equally to this work.

*Correspondence:
Yushun Gao
ysgaopumc@163.com
Shanqing Li
lishanqing@pumch.cn

Full list of author information is available at the end of the article

Keywords Adenocarcinoma of lung, Long-chain-fatty-acid-CoA ligase, Prognosis, Lymphatic metastasis, Tumor microenvironment

Introduction

Lung adenocarcinoma (LUAD) is marked by high lymph node metastasis (LNM) rates, contributing to disease recurrence and reduced survival [1–4]. Emerging evidence highlights metabolic reprogramming—particularly fatty acid metabolism (FAM)—as a critical contributor to LNM [5–7]. Tumor cells utilize FAM for energy production, membrane biosynthesis, and prometastatic signaling, yet the roles of FAM-related genes in LUAD LNM are not well understood [8–10].

Previous studies revealed that FAM-related genes are dysregulated in metastatic LUAD. Overexpression of ATP citrate lyase (ACLY) is associated with advanced stages, lower pathological grades, and poorer prognoses [11]. Mechanistically, FAM promotes LNM through β-oxidation-driven ATP production to fuel invasive cell migration and the secretion of lipid metabolites (e.g., prostaglandin E2) that upregulate VEGF-C in lymphatic endothelial cells, thereby inducing lymphangiogenesis [12–14]. Despite these advances, systematic analyses linking FAM-related genes to LNM and prognosis prediction of LUAD patients are lacking.

We combined transcriptomic and single-cell RNA sequencing (scRNA-seq) data from the two public databases to identify FAM-associated genes linked to LNM and prognosis in LUAD patients. A FAM-based prognostic model was developed, and its associations with gene mutations and tumor microenvironment (TME) characteristics were analyzed. Furthermore, we explored the effects of ACSL3 through cellular assays and tissue validation.

Materials and methods

Transcriptomic data acquisition and processing

We selected RNA expression profiles and corresponding clinical data from the TCGA database for LUAD (n = 513) to construct the model. Datasets from the GEO database with more than 50 samples, including GSE81089, were used as RNAseq validation cohorts. LUAD datasets from GEO datasets with over 50 samples, specifically GSE13213, GSE14814, GSE26939, GSE30219, GSE31210, GSE37745, GSE42127, GSE50081, GSE68465, and GSE72094, were utilized as validation sets. Microarray dataset normalization was conducted by 'limma' package.

Acquisition and processing of scRNA-seq data

Single-cell seq datasets GSE189357 and GSE235782 were obtained from the GEO database and processed with the 'seurat' package. Cells with mitochondrial content below 20% underwent quality control. Data preprocessing steps, including normalization, variable feature identification, and scaling, were performed using NormalizeData, FindVariableFeatures, and ScaleData functions, respectively. Batch effect correction was achieved with the "harmony" algorithm. Subsequently, dimensionality reduction and clustering were implemented using UMAP, tSNE and Louvain algorithm. To discover differentially expressed genes (DEGs) across clusters or cell types, the FindAllMarkers function was employed, applying the thresholds: p-value < 0.05, $\log_2$ fold-change (log2FC) > 0.25, and minimum expression proportion > 0.1.

Identification of genes associated with FAM

Genes related with FAM were sourced from the KEGG database (https://www.genome.jp/brite/hsa00001). This study identified 19 genes: ACAC family (ACAC A, B), ACSF3, NDUFAB1, MCAT, FASN, OXSM, CBR4, HSD17B8, HTD2, MECR, OLAH, ACSL family (ACSL1, 3, 4, 5, 6, BG1, and BG2).

NMF cluster analysis

Nonnegative matrix factorization (NMF) was applied to the 19 FAM reprogramming-related genes in the TCGA-LUAD datasets, using the NMF function from the NMF package with nrun = 50 and default parameters for all other settings.

Cell annotation analysis

We initially employed markers for various cell types: epithelial cells ("EPCAM", "KRT18", "KRT19", "CDH1"), fibroblasts ("DCN", "THY1", "COL1A1", "COL1A2"), endothelial cells ("PECAM1", "CLDN5", "FLT1", "RAMP2"), T cells ("CD3D", "CD3E", "CD3G", "TRAC"), NK cells ("NKG7", "GNLY", "NCAM1", "KLRD1"), B cells ("CD79A", "IGHM", "IGHG3", "IGHA2"), myeloid cells ("LYZ", "MARCO", "CD68", "FCGR3A"), and mast cells ("KIT", "MS4A2", "GATA2"). Visualizations were generated on the basis of these markers.

Calculation of the fatty acid metabolism-related gene score and construction of the risk model (Fscore)

We performed a univariate Cox regression analysis on nineteen genes related with the reprogramming of FAM and found 5 genes linked to prognostic risk and 1 gene with protective properties (P < 0.05). The risk signature, comprising five prognostic genes, was evaluated using the Fscore calculated through 'GSVA' package, with parameters set to method = "ssgsea", kcdf = "Gaussian", min.sz = 1, and ssgsea.norm = TRUE. In the TCGA dataset, risk groups were divided using the median value, while in

other validation datasets, the surv_cutpoint algorithm of 'survminer' package was applied.

Examination of immune and DNA damage attributes

Immune infiltration was evaluated using the "MCP-counter" R package, which measures the abundance of microenvironment cell populations (MCPs). The gene expression profile (GEP) score and The Cytolytic activity (CYT) score for each sample was calculated via the GEP gene signatures by GSVA algorithm. Data on immune checkpoint genes, T/B cell receptor richness, aneuploidy, homologous recombination deficiency, and LOH_n_seg were sourced from the publication [15]. Pathway scores for cancer hallmarks were computed using the "IOBR" package.

Spatial transcriptomics data analysis

Cell annotation was performed using the CellTrek package based on the cell type annotations derived from single-cell data, following the tutorial and parameter settings available at https://github.com/navinlabcode/CellTrek. The Fscore was also calculated using the ssGSEA algorithm with parameters kcdf = "Gaussian", min.sz = 1, and ssgsea.norm = TRUE. Visualization of spatial transcriptomics data was carried out using the Seurat package.

Tissues and immunohistochemistry (IHC)

Following ethical approval, 98 pairs of formalin-fixed paraffin-embedded (FFPE) LUAD tumor tissues and normal tissues were collected from patients who underwent resection at Cancer Hospital, Chinese Academy of Medical Sciences and Peking Union Medical College between January 2019 and December 2020. Overall survival (OS) was calculated from follow-up data up to August 2024, with clinical parameters extracted from hospital records. ACSL3 expression was evaluated semiquantitatively through IHC using anti-ACSL3 (ab151959, 1:500, Abcam) and an HRP-conjugated secondary antibody (ab205718, 1:5000, Abcam), followed by DAB visualization. Blinded observers independently scored staining intensity (0–3) and positive cell proportion (0–4), with composite scores categorized into low or high expression groups. Four sample pairs with staining failure were excluded, yielding 94 pairs that could be used to evaluate the correlation of ACSL3 expression with clinical outcomes.

Cell culture and transfection

A549 and PC-9 LUAD cells (National Collection of Authenticated Cell Cultures, Shanghai) were cultured in RPMI-1640 with 10% FBS (Gibco), while human lymphatic endothelial cells (HLECs; ScienCell) were maintained in endothelial cell medium (ScienCell), both under 5% CO_2 at 37 °C. For transfection, cells seeded in 6-well plates (5×10^5 cells/well, ~80% confluence) were transfected with ACSL3-shRNA (sh-ACSL3) or ACSL3-overexpressing plasmids (OE-ACSL3) (GenePharma) via Lipofectamine 3000 (Life Technologies). Forty-eight hours after transfection, the medium was refreshed with complete medium.

Western blot

Cells were lysed in RIPA buffer (Beyotime) supplemented with protease inhibitors and PMSF, and protein concentrations were determined using a BCA assay (Beyotime) prior to SDS–PAGE separation and PVDF membrane transfer. Membranes were blocked with Western BLoT buffer (Takara) and incubated at 4 °C with primary antibodies for about 10 h: ACSL3 (ab151959, 1:500, Abcam), FASN (ab128870, 1:10000, Abcam), ACC (ab109368, 1:5000, Abcam), ACLY (ab126129, 1:5000, Abcam), VEGF-C (22601-1-AP, 1:1000, Proteintech), c-Myc (ab32072, 1:1000, Abcam), GAPDH (ab9485, 1:2500, Abcam), and β-actin (ab115777, 1:500, Abcam). Protein bands were visualized using enhanced chemiluminescence (ECL) reagents (Thermo Fisher) after incubation with an HRP-conjugated secondary antibody (ab205718, 1:5000, Abcam) for 2 h at room temperature.

Cellular functional assays

In scratch wound healing assays, confluent monolayers of transfected cells were linearly scratched using sterile pipette tips, washed with PBS, and cultured in 1% FBS/RPMI-1640 to limit proliferation. Migration was monitored via inverted microscopy (Nikon) at 0 and 24 h, and scratch closure was quantified via ImageJ (National Institutes of Health, USA).

Transwell invasion assays utilized Matrigel-coated chambers (BD Biosciences) containing 2×10^4 serum-starved A549 or PC-9 cells in the chambers, with 10% FBS/RPMI-1640 serving as the chemoattractant. After 24 h of incubation, membranes were fixed with 4% PFA, stained with 0.1% crystal violet, and invading cells were counted in five 200× fields.

Cellular proliferation was assessed via a CCK-8 assay (Dojindo). Cells (5×10^3 per well) in 96-well plates were incubated with CCK-8 for 2 h at intervals of 0, 24, 48, and 72 h, followed by absorbance measurement at 450 nm using a Bio-Rad microplate reader.

Apoptosis was assessed using Annexin V-FITC/propidium iodide (PI) staining (BD Biosciences) and subsequent flow cytometry. The transfected cells were resuspended in binding buffer, dual-stained, and analyzed within 1 h.

Endothelial cell tube formation assays

The serum-free medium obtained from the tumor cells was concentrated 10-fold via ultrafiltration centrifugal

devices (Millipore, Billerica, MA, USA). HLECs were subsequently seeded into Matrigel-precoated 6-well plates and cultured with concentrated medium for 6 h. Lymphatic capillary structures were visualized via inverted microscopy, and the lengths of the tubular structures were quantitatively analyzed via ImageJ software.

Triglyceride and phospholipid quantification

Cellular triglycerides and phospholipids were measured in various groups using the EnzyChrom™ Triglyceride and Phospholipid Assay Kits (BioAssay Systems). The working reagent (90 μL per well) was dispensed into a 96-well plate containing processed samples. The plates were gently tapped for mixing and incubated for half hour at room temperature, shielded from light. Finally, absorbance was recorded at 570 nm.

Statistical analysis

Computational processing, quantitative analyses, and graphical representations were conducted with R (v4.1.3) and GraphPad Prism 9.5. The associations for metric data were evaluated through Pearson correlation analysis. Groupwise comparisons employed χ^2 testing for categorical data, while Wilcoxon rank-sum tests or t-tests addressed continuous variables. Optimal thresholds were established using the 'survminer' package. Survival outcomes were evaluated via proportional hazards regression and Kaplan-Meier methods.

Results

Relationships between prognosis and FAM-related genes in LUAD

We obtained 19 FAM-related genes from the KEGG database to investigate their role in LUAD. The expression correlation of these genes is shown in Supplementary Figs. 1A-B. We conducted NMF clustering analysis (Supplementary Figs. 1C-D) and found that the best clustering effect was achieved with k = 4. LUAD patients were categorized into four groups, and a heatmap of the 19 gene expression levels was generated. The analysis showed that OLAH genes were predominantly expressed in Cluster 3, while ACSBG1 genes were more highly expressed in Cluster 2 (Fig. 1A). Further prognostic analysis of Clusters 1–4 revealed significant differences in outcomes, with the best prognosis in Cluster 2 and the worst in Cluster 3 (Fig. 1C). Univariate Cox regression analysis on 19 LUAD-related genes identified 6 genes significantly affecting overall survival (OS) in LUAD patients. Five of these, ACSL3, MCAT, NDUFAB1, OLAH, and ACSL4, were risk factors and all associated with FAM activation (Fig. 1B). Thus, we identified these genes as a signature gene set indicative of FAM activity and prognostic prediction and further analyzed the expression correlation of these five risk genes (Supplementary Fig. 1E).

Using the ssGSEA algorithm, we developed a FScore on the basis of the five identified risk genes. The FScore exhibited significant inter-cluster variation, with Cluster 2 showing the lowest and Cluster 3 the highest values (Fig. 1C-D). In the TCGA cohort, patients with an Fscore above the median exhibited significantly poorer prognosis, a trend consistently confirmed in three independent GEO datasets (GSE13213, GSE26939, GSE37745). Multivariate Cox analysis validated the Fscore as an independent prognostic biomarker, underscoring its robustness in stratifying LUAD outcomes (Supplementary Fig. 2A-D).

Relationships between the FAM and LNM in LUAD

To investigate the association of FAM with LNM in LUAD, we analyzed TCGA lymph node-negative (N0) versus positive (N1/N2) cohorts and identified the differential expression of 19 FAM-related genes (e.g., *NDUFAB1* and *MCAT* were downregulated at N0; *ACACB* and *ACSF3* were upregulated at N0; Fig. 2A-B). Consistently, FScore was lowest in N0, and it progressively increased with nodal stage (N0 < N1 < N2; Fig. 2C–D). Notably, a high FScore predicted a poor prognosis in both the N0 subgroup and the N+ subgroup (Fig. 2E-F), indicating that FAM activation not only correlates with poor outcomes but also may directly drive lymphatic dissemination. Further, DEGs analysis was performed between the high-FScore and low-FScore groups (Fig. 2G), followed by overrepresentation analysis (ORA) based on the GO and KEGG databases. The results showed that the DEGs were primarily enriched in metabolic pathways and extracellular matrix-related pathways (Fig. 2H-I). Subsequently, GSEA was conducted on the gene sets of the two groups, revealing that the high-score group exhibited significant enrichment in four pathways: HALLMARK_OXIDATIVE_PHOSPHORYLATION, HALLMARK_MTORC1_SIGNALING, HALLMARK_MYC_TARGETS_V1, and HALLMARK_ADIPOGENESIS (Fig. 2J). Notably, the mTORC1 and Myc pathways are classic oncogenic pathways, which partially explains the poor prognosis observed in the high-FScore group.

Relationships between the FScore and gene mutations in LUAD

The mutation burden of LUAD includes actionable driver mutations (e.g., EGFR, KRAS) and immunotherapy-predictive alterations, which has a significant impact on the TME and the response to immunotherapy [16, 17]. We investigated the interplay of FAM with these mutations and observed distinct patterns: FLG, LRP1B, USH2A, and STK11 mutations were enriched in low-FScore patients, whereas targetable EGFR/KRAS mutations were not associated with FScore (Figs. 3A-B; Supplementary Figs. 3 A-S). Notably, LRP1B/STK11—established

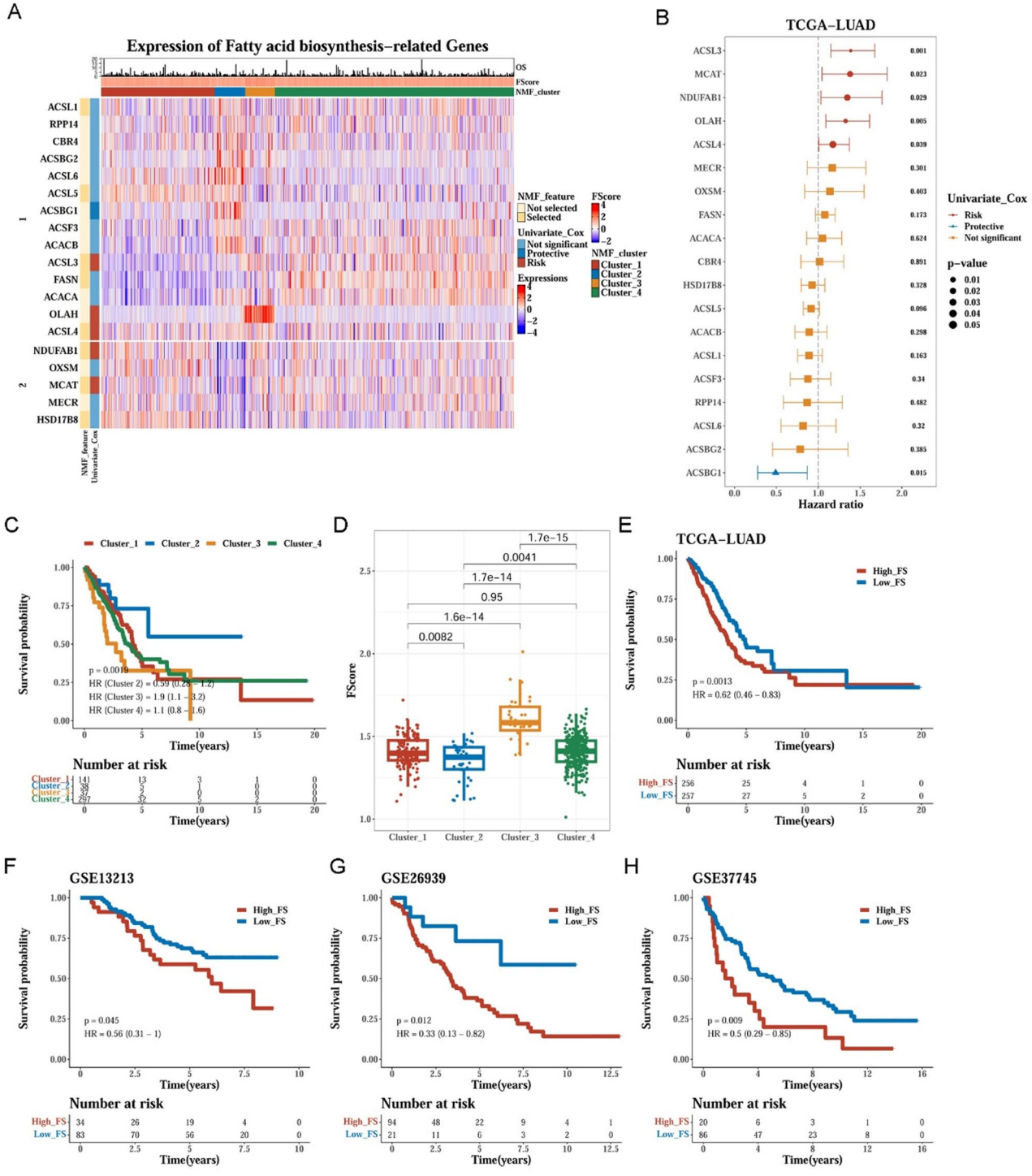

Fig. 1 Analysis of FAM-related genes' prognostic significance in LUAD. **A** Expression profiles of 19 FAM-related genes in different NMF clusters of the TCGA-LUAD cohort; red and blue tones correspond to increased and reduced levels of expression, sequentially. **A** The x-axis denotes patients, while the y-axis indicates genes. **B** Univariate Cox analysis is conducted on 19 FAM-related genes. **C** Survival analysis is performed on four groups identified by the NMF algorithm. **D** Differences in FScore value distribution are examined across the four clusters. **E** Survival analysis compares the high-FScore group to the low-FScore group. **F**-**H**. Survival analyses based on different FScore groupings in three public GEO datasets (GSE13213, GSE26939, and GSE37745)

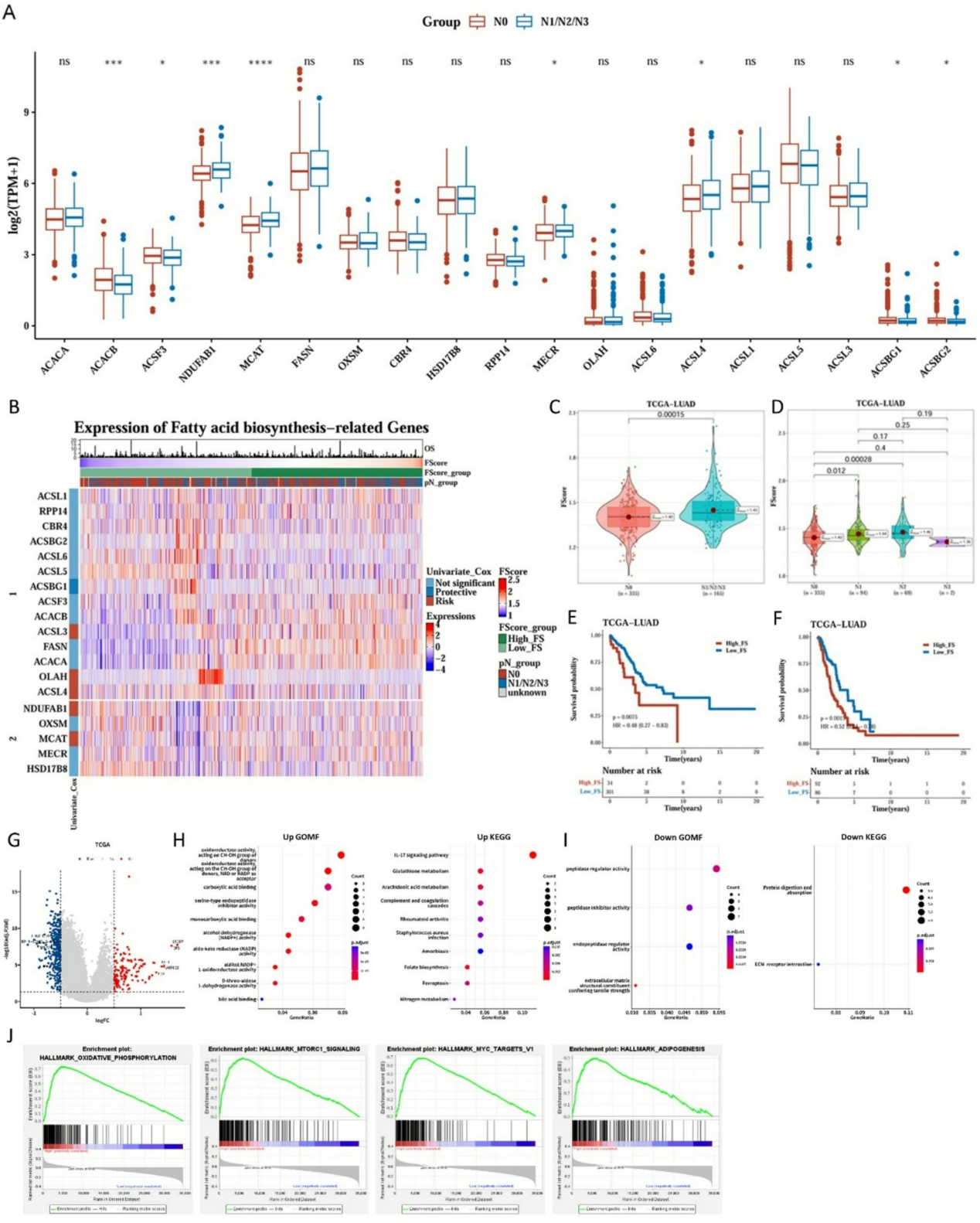

Fig. 2 (See legend on next page.)

(See figure on previous page.)

Fig. 2 Correlations between FAM and LNM. **A** Analysis of 19 FAM-related gene expressions in lymph node (-) and lymph node (+) groups within the TCGA cohort. **B** Expression profiles of 19 FAM-related genes in TCGA patients are shown with corresponding N stage, where red and blue tones correspond to increased and reduced levels of expression, sequentially. The x-axis denotes patients while the y-axis indicates genes; **C**. FScore distribution in lymph node (-) versus lymph node (+) groups; **D**. FScore distribution across stages N0, N1, N2, and N3; **E**-**F**. Survival analysis of varying FScore risk groups within lymph node-negative and lymph node-positive categories; **G**. analysis of DEGs between two risk groups; **H**. ORA analysis in elevated DEGs; **I**. ORA analysis in downregulated DEGs; **J**. The results of GSEA analysis

immunotherapy response markers in NSCLC [18–20]—were linked to a low Fscore, suggesting enhanced immunotherapeutic potential in this subgroup. Furthermore, FLG-mutant LUAD patients exhibited both a reduced FScore (Fig. 3C) and improved survival (P = 0.0081, Fig. 3D).

Relationships between the FScore and immune cell infiltration

To explore the relationships between FScore and immune cell infiltration, associations between the FScore and the enrichment of 50 MSigDB hallmark gene sets were evaluated. The FScore exhibited strong positive correlations with lipid metabolic pathways (e.g., fatty acid oxidation and oxidative phosphorylation) and negative associations with apoptosis/DNA repair across the 12 LUAD cohorts (Fig. 4A). Strikingly, high FScore tumors displayed immunosuppressive features, including reduced T/B cell infiltration (MCP-counter; Fig. 4B-C), downregulated immune checkpoints (CXCL9, ICOS; Fig. 4D), and suppressed cytolytic activity (CYT), T cell receptor (TCR/B) clonality, and inflamed gene signatures (Fig. 4E-F). The results indicate that FAM-driven metabolic changes lead to an 'immune-cold' phenotype, while a low FScore is associated with an immunogenic 'hot' microenvironment, marked by enhanced antigen presentation and effector immune activation, potentially offering a survival benefit to patients with a low FScore.

Heterogeneity of FAM in the TME across multi-omics

Considering the relationships between FAM and TME, we examined the FScore distribution across four TME subtypes, which are key immunotherapy biomarkers in various cancers: 'Immune-exhausted' (D), 'Fibrotic' (F), 'Immune-enriched, non-fibrotic' (IE), and 'Immune-enriched, fibrotic' (IE/F). The results revealed that D-TME tumors presented the highest FScore in the six LUAD cohorts (Fig. 5A), which aligns with their classification as immunotherapy-resistant "cold" tumors. Single-cell resolution analysis further demonstrated cell type-specific FAM activity. The epithelial, mast, and myeloid cells presented elevated FScore in both the GSE189357 (Fig. 5B-C) and GSE235782 datasets (Fig. 5D-E), with consistent expression patterns of core FScore genes (ACSL3, MCAT, etc.; Supplementary Fig. 4A-B). These findings highlight the functions of FAM in sculpting the immunosuppressive TME and driving metabolic reprogramming in discrete cellular niches.

Spatial transcriptomics mapped FAM heterogeneity across the TME landscape, overcoming scRNA-seq's spatial limitations. Fibroblasts and myeloid cells spatially proximal to tumor niches presented elevated FScore (Fig. 5F).Interestingly, FScore was highly enriched in epithelial cells, mast cells, and myeloid cells, mirroring the single-cell findings (Fig. 5H). Notably, core FAM genes (ACSL3, MCAT, etc.)displayed cell type-specific spatial expression patterns congruent with the FScore distribution (Supplementary Fig. 5), collectively underscoring metabolic reprogramming as a spatially orchestrated process across TME cellular compartments.

High expression of ACSL3 is an independent prognostic risk factor related to advanced TNM stage

To investigate the mechanism linking Fscore and LUAD, we focused on ACSL3, the gene with the most significant prognostic impact on Fscore. According to the GEPIA2 online database, ACSL3 is overexpressed in LUAD and correlates with poor prognosis (Fig. 6A). IHC revealed markedly elevated ACSL3 expression in malignant versus adjacent tissues (Fig. 6B). High ACSL3 expression was associated with significantly reduced overall survival, and ACSL3 was independently associated with worse prognosis in LUAD patients based on multivariate Cox regression (Fig. 6C). A greater proportion of patients with low differentiation, high T stage and high N stage had high expression of ACSL3 (Fig. 6D).

ACSL3 activates FAM and promotes HLEC tube formation as well as malignant biological behaviors via the c-Myc pathway

We overexpressed and knocked down ACSL3 in LUAD cells and verified the efficiency of the intervention by western blotting (Fig. 7A). To investigate ACSL3-mediated lipid homeostasis, intracellular triacylglycerol (TAG) and phospholipid (PL) levels were quantified. The overexpression of ACSL3 in A549 cells increased intracellular TAG and PL levels and upregulated key FAM enzymes (FASN, ACC and ACLY), whereas the knockdown of ACSL3 suppressed these effects (Fig. 7B and C). The results indicate that ACSL3 is crucial for cellular FAM. Furthermore, we found that the overexpression of ACSL3 enhanced malignant phenotypes, including cell migration, invasion, and proliferation (Fig. 7E-G), promoted

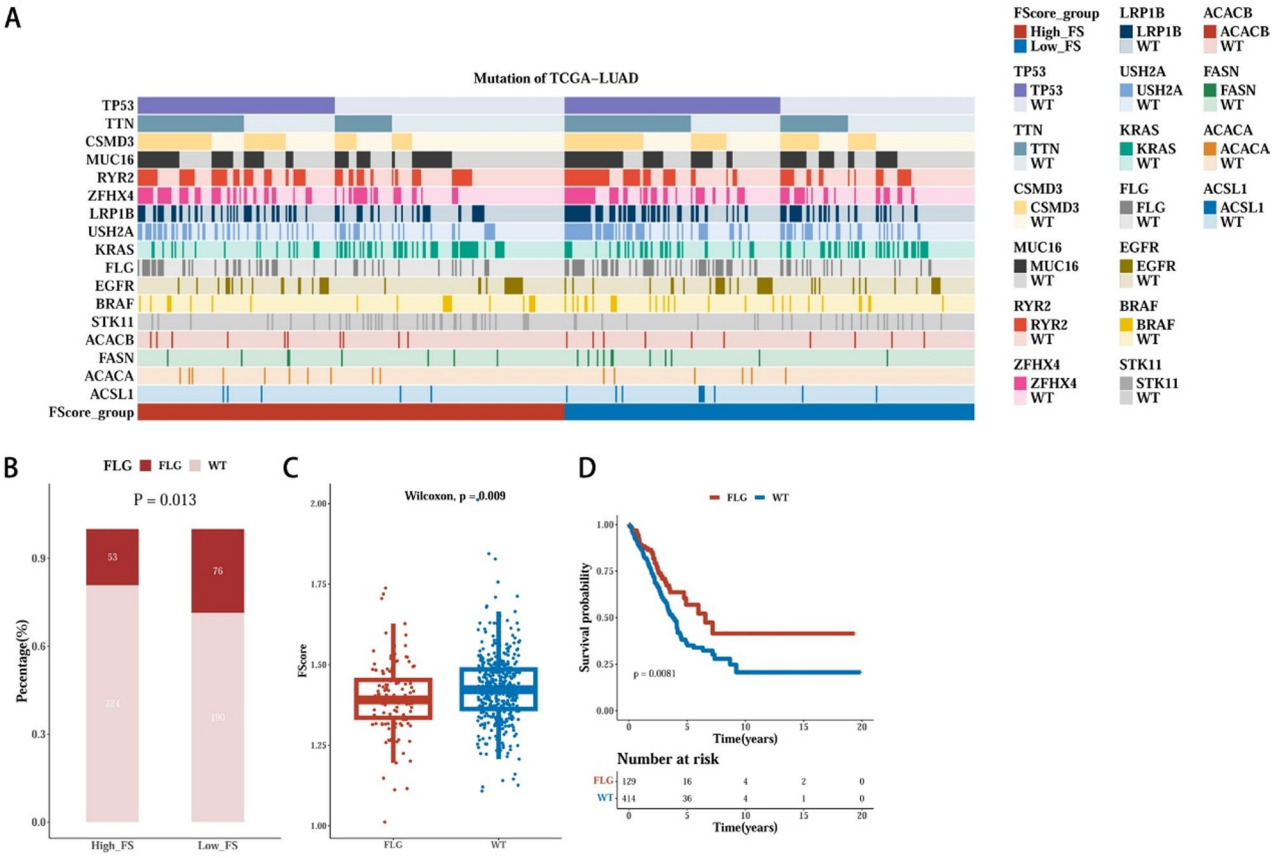

Fig. 3 Correlations between the FScore and gene mutations. **A** Mutation statuses across FScore groups within the TCGA-LUAD cohort. **B**-**C** Analysis of the TCGA-LUAD cohort reveals distinctions in FScore between groups with and without FLG mutations. **D** survival outcomes are assessed based on FLG mutation status

HLEC tube formation (Fig. 7D), and reduced apoptosis (Fig. 7H).

An integrated analysis of the TCGA database and GSEA analysis indicated significant enrichment of ACSL3 high-expression phenotypes in fatty acid metabolism and MYC signaling pathways (Fig. 7I). Prior evidence established c-Myc as a transcriptional activator of VEGFC, namely, a pivotal lymphangiogenic factor, through direct E-box binding to the VEGFC promoter [21]. The western blot results revealed that overexpression of ACSL3 upregulated c-Myc and its downstream lymphangiogenic factor VEGFC (Fig. 7J), establishing an ACSL3/c-Myc/VEGFC axis that promotes lymphatic metastasis.

Discussion

This study systematically delineates the prognostic and mechanistic roles of FAM reprogramming in LUAD, with a focus on its interplay with LNM and TME remodeling. We developed FScore as a reliable biomarker for prognosis and nodal dissemination by integrating multiomics data from bulk, single-cell, and spatial transcriptomics. Furthermore, functional validation identified ACSL3 as a key gene involved in FAM-mediated metabolic reprogramming and lymphatic metastasis, revealing a novel ACSL3/c-Myc/VEGFC regulatory axis. These findings advance our understanding of metabolic plasticity in LUAD progression and offer actionable insights for therapeutic targeting.

Our identification of a 5-gene FAM-related signature (ACSL3, MCAT, NDUFAB1, OLAH, ACSL4) highlights the clinical relevance of FAM in LUAD, corroborating recent studies identifying FAM as a conserved vulnerability in malignancies [22]. The FScore model demonstrated consistent prognostic power across 12 independent cohorts, and FScore escalation was correlated with advanced nodal stage (N0 < N1 < N2; Fig. 2C-D), which implied the activation of the FAM in LUAD patients with LNM. Choong-Kun Lee's study mechanistically supports this phenomenon by showing that LNM necessitates a metabolic shift towards fatty acid oxidation in tumor cells, as observed in preclinical models [5].

Numerous studies have confirmed that tumor metabolism has a significant impact on the "cold" or "hot" phenotype of the TME and is closely associated with antitumor immune responses [23, 24]. The association of a high FScore with the immunosuppressive TME features—reduced T/B cell infiltration and downregulated checkpoints—aligns

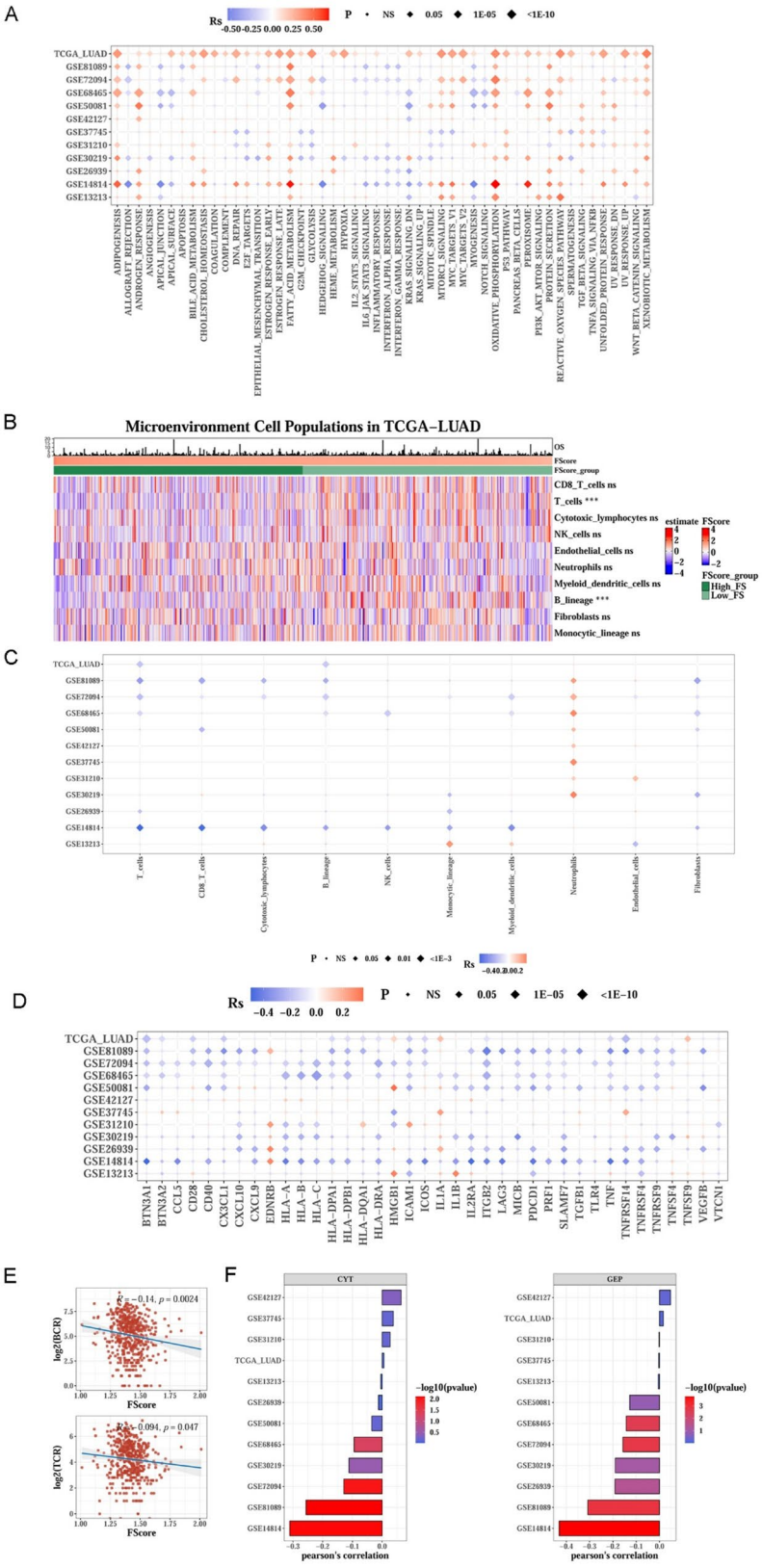

Fig. 4 FScore is related to immune cell infiltration. **A** Correlation of the Fscore with signaling pathways across 12 LUAD cohorts; **B**. Microenvironmental cell population infiltration levels in various FScore groups of TCGA-LUAD patients; **C**. Correlation between FScore and immune cell infiltration; **D**. FScore correlation with immune checkpoint gene expression across 12 LUAD cohorts; **E**. FScore correlation with TCR/BCR richness in TCGA-LUAD patients; **F**. FScore correlation with cytotoxicity markers CYT and GEP

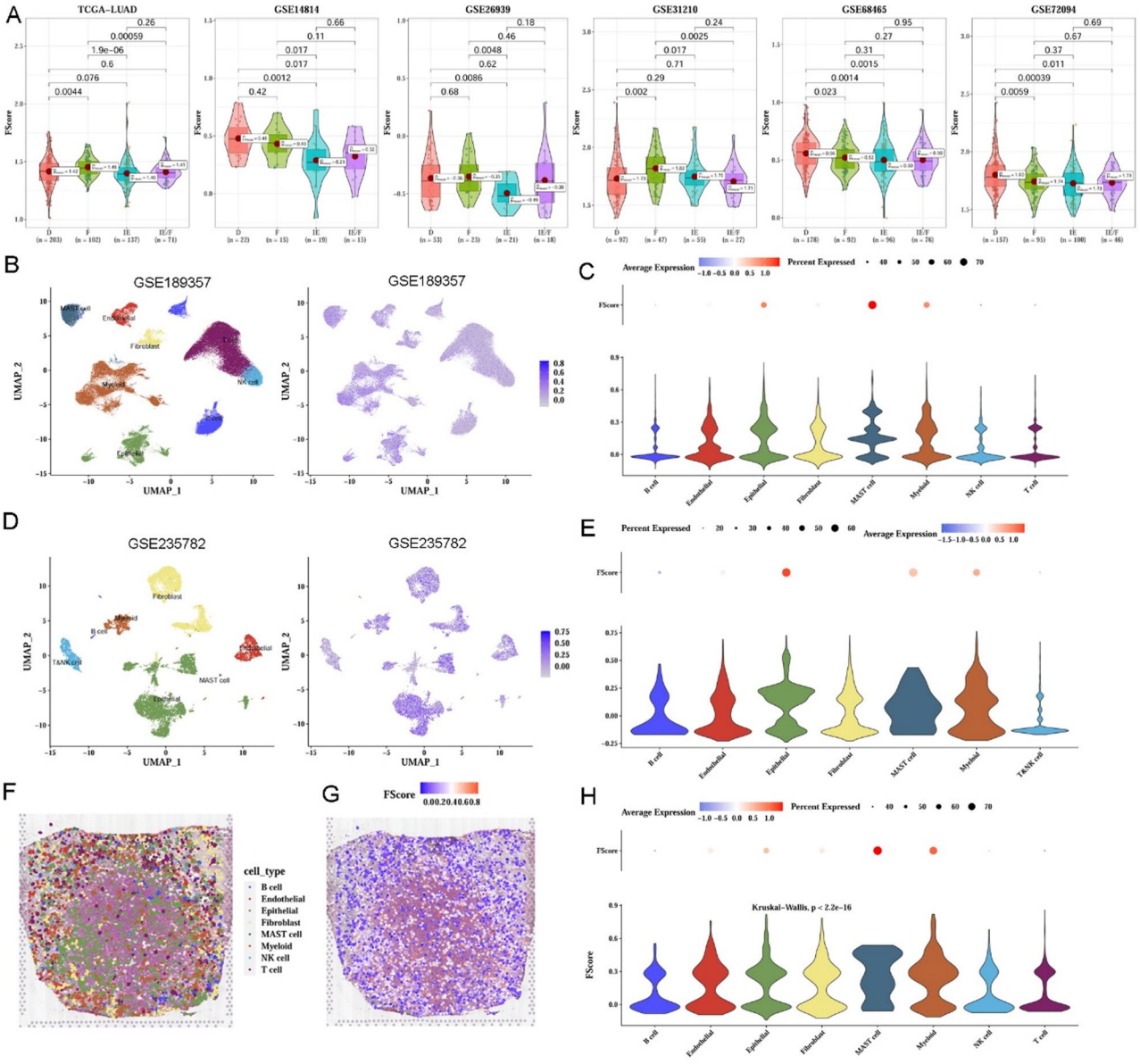

Fig. 5 Diversity of FAM within the TME at multiple transcriptomic resolutions. **A** FScore across various TME subtypes in six datasets; **B** and **D**. Dimensionality and feature reduction of the FScore in two LUAD scRNA-seq datasets. Consistent colors represent matched cell types across datasets; **C** and **E**. FScore among cell types. Identical color coding is applied to both cell types and their counterparts in the dimensionality reduction plots to the left. For the dot plots, the legend's blue to white to red gradient represents a low to high transition in the FScore, with the dot size indicating the expression proportion; **F**. Cell type identification in spatial transcriptomics data. The entire tissue section is mapped for eight distinct cellular populations. Panel **G** displays the FScore for each cell type in the spatial transcriptomics data. Panel **H** shows the FScore for various cell types, aligning with the results in Panels **C** and **E**. The x-axis indicates the number of cell types, while the y-axis represents the FScore

with the evidence that activated FAM impedes antitumor immune responses [25, 26]. Our multiomics analysis revealed unprecedented spatial and cellular specificity of FAM activity. Spatial transcriptomics complemented scRNA-seq to resolve FAM heterogeneity, revealing elevated FScore in tumor-proximal fibroblasts/myeloid cells and epithelial/mast/myeloid niches, with core FAM genes (e.g., ACSL3 and MCAT) exhibiting cell type-specific spatial patterns that underscore spatially orchestrated metabolic reprogramming across TME compartments. This spatial orchestration suggests that FAM-driven metabolic crosstalk between malignant and stromal compartments is potentially mediated by lipid metabolites that reprogram adjacent cells [27]. This heterogeneity may explain why global FAM inhibition has yielded limited clinical success, emphasizing the need for cell type-specific targeting strategies.

Given the predominant impact of ACSL3 on the FScore, ACSL3 was prioritized for further mechanistic

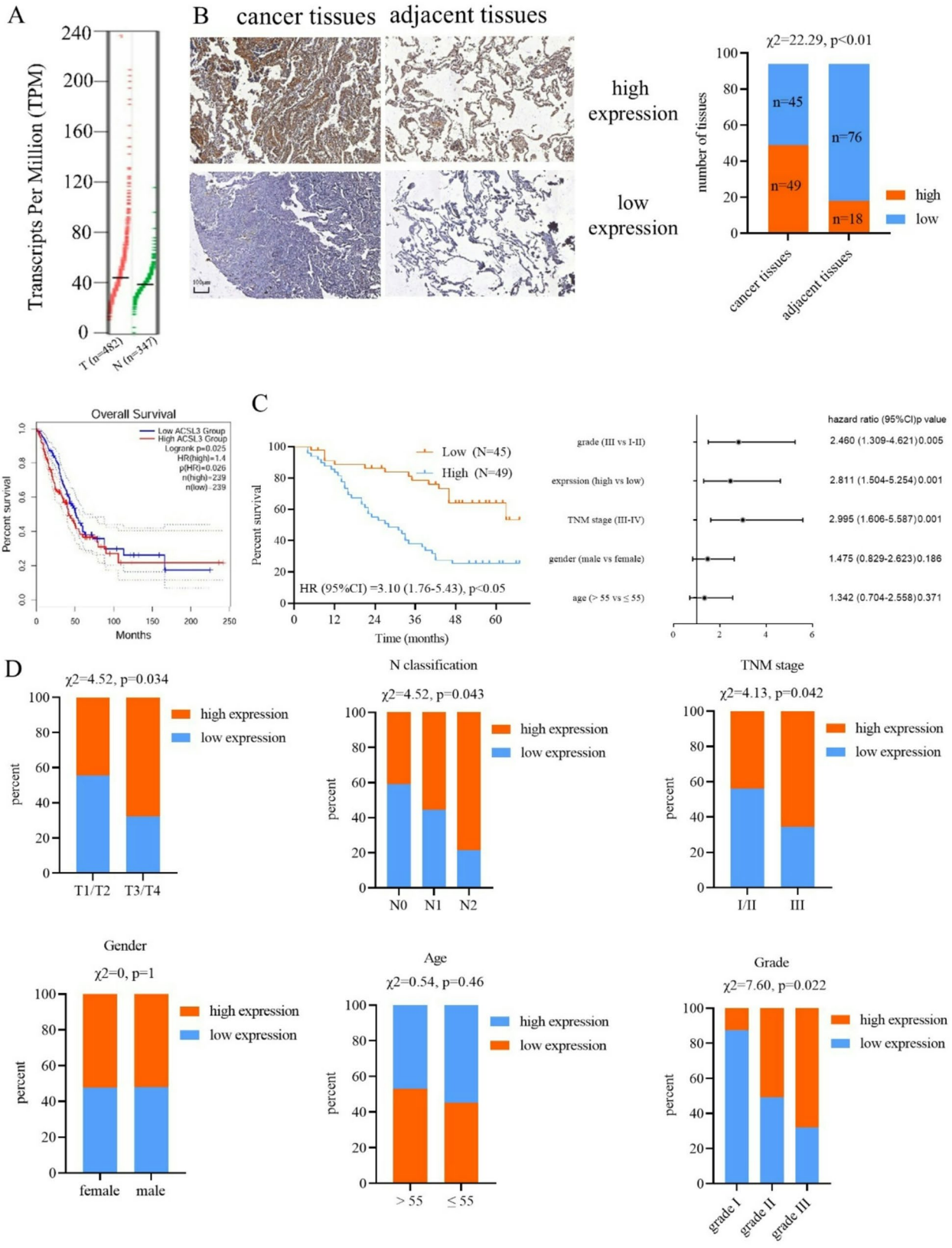

Fig. 6 Relationships between ACSL3 expression and clinical characteristics. **A** The GEPIA2 online database was utilized to assess ACSL3 expression in LUAD and normal tissues, as well as its prognostic impact. **B** Images of IHC and expression of ACSL3 in 94 pairs of LUAD and adjacent tissues (bar=100 μm); **C**. Effects of ACSL3 expression on prognosis evaluated by Kaplan–Meier curves and multivariate Cox regression; **D**. Correlations between ACSL3 expression and T classification, N classification, TNM stage, gender, age and grade.

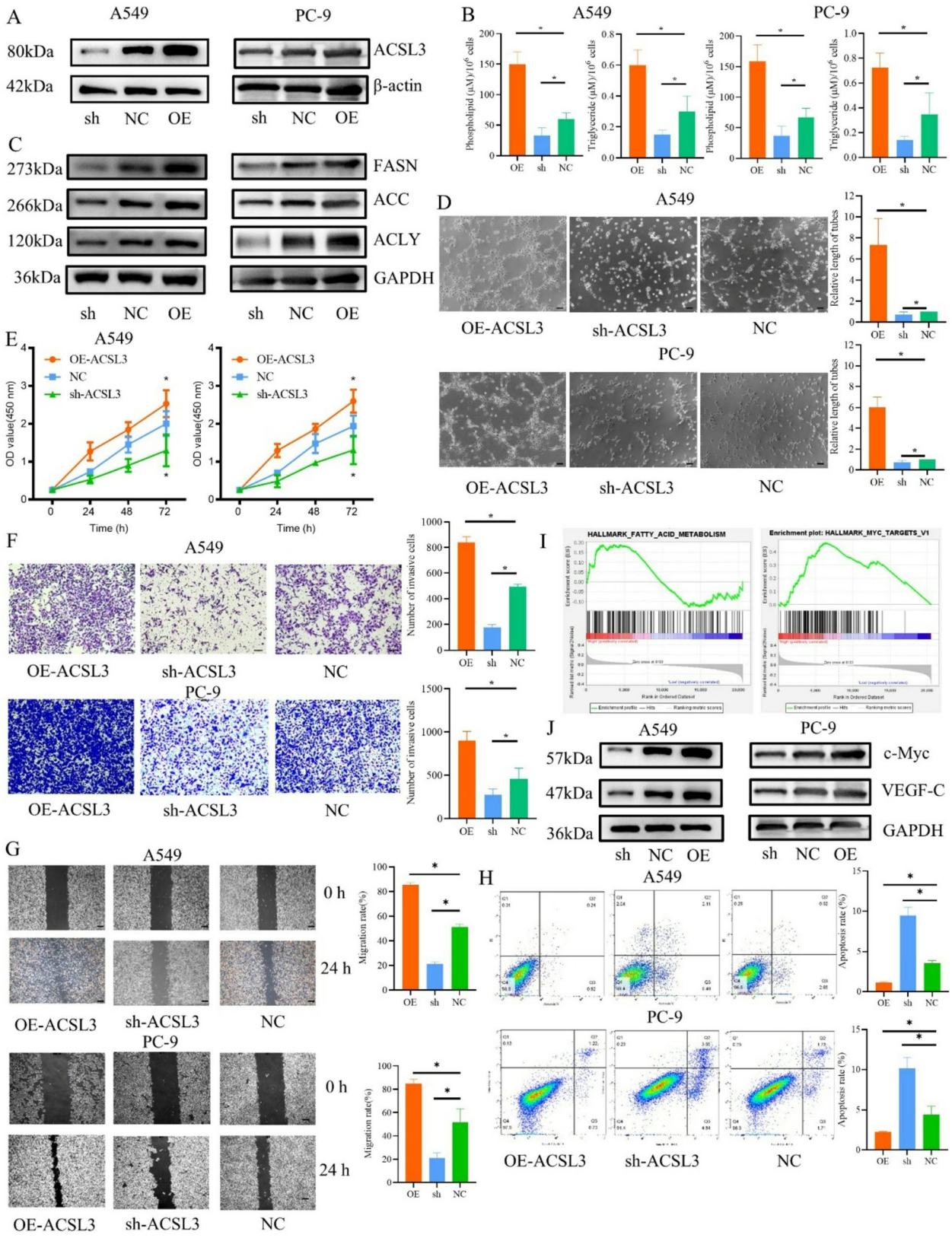

Fig. 7 (See legend on next page.)

(See figure on previous page.)

Fig. 7 Effects of ACSL3 on the cellular functions of LUAD and its mechanism. **A** The efficiency validation of the intervention of ACSL3 by western blot; (**B**) The TAGs and PLs levels in OE-ACSL3 group and sh-ACSL3 group; (**C**) The expressions of FAM enzymes in OE-ACSL3 group and sh-ACSL3 group; (**D**) The HELCs tube formation in OE-ACSL3 group and sh-ACSL3 group (bar=100 μm); (**E**) The CCK-8 assays in OE-ACSL3 group and sh-ACSL3 group; (**F**) The invasion assays in OE-ACSL3 group and sh-ACSL3 group (bar=100 μm); (**G**) The Wound Healing assays in OE-ACSL3 group and sh-ACSL3 group (bar=200 μm); (**H**) The apoptosis assays in OE-ACSL3 group and sh-ACSL3 group; (**I**) The Gene Set Enrichment Analysis of ACSL3; (**J**) The expression of c-Myc and VEGF-C in OE-ACSL3 group and sh-ACSL3 group

investigation. ACSL3 promotes tumor cell proliferation and metastasis by enhancing resistance to lipid peroxidation and ferroptosis through increasing monounsaturated fatty acid (MUFA) levels or the uptake of oleic acid [28–33]. Mechanistically, ACSL3 activates the PPARα signaling pathway via 1-palmitoyl-2-oleoyl-sn-glycero-3-phosphocholine synthesis, accelerating lipid catabolism and anabolism to fuel cancer progression [34]. Furthermore, ACSL3 collaborates with LPIAT1 to remodel phosphatidylinositol species, driving prostaglandin synthesis to promote tumor progression and immune evasion [35]. In pancreatic ductal adenocarcinoma, ACSL3 upregulates plasminogen activator inhibitor-1 (PAI-1) secretion, stimulating tumor and stromal cell proliferation, amplifying immunosuppressive cell infiltration, and reducing cytotoxic T-cell recruitment [36]. In NSCLC, ACSL3 promotes mitochondrial β-oxidation and epithelial–mesenchymal transition (EMT) by activating long-chain fatty acid metabolism, which enhances proliferation, migration, and invasion [37]. Furthermore, a recent study has reported the establishment of a lipid metabolism-related prognostic signature and identified ACSL3 as a key regulator of immunotherapy response and immune evasion of LUAD [38]. However, the role of ACSL3 in lymphatic metastasis remains to be elucidated.

Our study pinpointed ACSL3 as an effector of FAM and lymphangiogenesis in LUAD, which has not been reported before. ACSL3 overexpression amplified lipid pools (TAGs/PLs) and upregulated the expression of FAM enzymes, directly enhancing malignant phenotypes, including proliferation, invasion, and lymphangiogenesis. The mechanism by which ACSL3 influences LNM is undefined. However, research demonstrates that ACSL4, a paralog, sustains c-Myc oncoprotein levels via ERK/FBW7-mediated suppression of ubiquitin–proteasome degradation [39]. Elevated c-Myc activity augments SREBP1 transcription, resulting in higher expression of lipogenic enzymes. This cascade stimulates de novo lipid synthesis, including triglyceride/cholesterol production and lipid droplet biogenesis, thereby accelerating tumor growth [40]. In our study, we found that ACSL3 overexpression could upregulate the expression of c-Myc and VEGFC. Therefore, we believe that, mechanistically, ACSL3 activated c-Myc, a known transcriptional amplifier of VEGFC [21], thereby bridging metabolic reprogramming to lymphatic vessel formation. In addition, as an upstream regulator of fatty acid metabolism, ACSL3 promotes lymph node metastasis by enhancing lipid synthesis pathways (e.g., SREBP signaling) [41], synergistically with the c-Myc/VEGFC axis. A substantial body of evidence indicates that metastatic cancer cells depend on fatty acids for energy, membrane biosynthesis, and lipid signaling—all of which are essential for successful colonization in distant organs, including lymph nodes [5, 42, 43]. Moreover, elevated free fatty acids activate NF-κB and YAP signaling, upregulating the expression of factors such as TWIST1, MMP-9, and VEGFC, thereby inducing epithelial-mesenchymal transition and lymphangiogenesis to promote lymph node metastasis [7, 44–46].

Moreover, recent studies demonstrate that fatty acid metabolism influences invasiveness within dense matrices, blood vessels, and lymphatic vessels by modulating membrane fluidity, cell stiffness, and force generation [47–49]. Specifically, ACSL4 enhances membrane fluidity via polyunsaturated fatty acid synthesis to facilitate hematogenous extravasation [47], while SCD1 and the TFEB-ERRα axis promote membrane fluidity, pseudopodia formation, and invasiveness, driving LNM and distant metastasis [48, 49]. The TME can also affect the invasive ability of tumor cells by influencing their fatty acid metabolism. For example, cancer-associated fibroblasts secrete unsaturated phosphatidylcholine to increase membrane fluidity in colorectal cancer cells [50], and matrix stiffness shifts cancer cell metabolism toward fatty acid utilization [51] or triggers hepatic stellate cell lipolysis to fuel fatty acid oxidation, enhancing tumor cell survival and migration in dense stroma [52]. Collectively, these findings position ACSL3 as a promising therapeutic target and underscore that fatty acid metabolism lies at the intersection of intracellular signaling and microenvironmental cues in metastatic progression.

The FScore model offers a clinically tractable tool for risk stratification. Its association with immunotherapy-predictive mutations (e.g., LRP1B/STK11) further suggests its utility in guiding therapies targeting immune checkpoints. However, limitations include the retrospective nature of public cohorts and the need for prospective validation of FScore. While our in vitro models established the prometastatic role of ACSL3, future studies using patient-derived organoids or in vivo models could better recapitulate TME interactions. Furthermore, we will employ lipidomics analysis as a key point in future study, to examine the effects of ACSL3 on the change of lipidomics and to explore how the change influences functional phenotypes and signaling pathway activation.

Conclusion

This study reveals that reprogramming of FAM is a key metabolic hallmark driving LNM and poor prognosis in LUAD. By developing and validating FScore, we establish a clinically applicable stratification tool that effectively predicts patient survival and LNM risk. Mechanistically, we identify ACSL3 as a core effector within the FAM pathway: it activates the c-Myc/VEGFC axis to promote lipid synthesis, malignant phenotypes, and lymphangiogenesis, thereby fueling lymphatic dissemination. Collectively, our findings link FAM reprogramming to the immunosuppressive tumor microenvironment and spatial metabolic heterogeneity in LUAD, and propose the ACSL3/c-Myc/VEGFC axis as a potential therapeutic target to suppress LNM, offering new insights for metabolic subtyping and precision intervention in LUAD.

Abbreviations

LUAD	Lung adenocarcinoma
LNM	Lymph node metastasis
FAM	Fatty acid metabolism
ACLY	ATP citrate lyase
scRNA-seq	Single-cell RNA sequencing
TME	Tumor microenvironment
NMF	Nonnegative matrix factorization
MCPs	Microenvironment cell populations
GEP	Gene expression profile
CYT	Cytolytic activity
IHC	Immunohistochemistry
FFPE	Formalin-fixed paraffin-embedded
OS	Overall survival
FScore	Fatty acid metabolism-related gene score
DEGs	Differentially expressed genes
HLECs	Human lymphatic endothelial cells
TAG	Triacylglycerol
PL	Phospholipid
PAI-1	Plasminogen activator inhibitor-1
EMT	Epithelial-mesenchymal transition

Supplementary Information

The online version contains supplementary material available at https://doi.org/10.1186/s12931-026-03671-w.

Supplementary Material 1: Supplementary Fig 1. A. Heatmap of gene expression associated with fatty acid metabolism reprogramming. B. Histogram depicting the count of genes significantly linked to those involved in the reprogramming of fatty acid metabolism. C. The results of NMF clustering, which is used to determine the number of categories. D. Heatmap of NMF consensus clustering. E. Heatmap of correlations for the 5 risk genes used to calculate the FScore. Supplementary Fig 2. Box plot of the FScore for 4 datasets (TCGA-LUAD, GSE57253, GSE153494, and GSE192714). Supplementary Fig 3. (A) Mutation landscape of the top 10 high-frequency mutations in cohort (B) Mutation landscape of FAM-related genes. C-S. FScore of different mutation statuses of common genes. Supplementary Fig 4. A-B. Expression of the five key genes in the two single-cell datasets. Supplementary Fig 5. A-E. Expression of the five key genes in the spatial transcriptomics data.

Acknowledgements

Not applicable.

Authors' contributions

Yicheng Liang was responsible for conceptualization, data curation, methodology, software, supervision, validation, and writing, including both the original draft and review and editing. Linchuan Liang contributed to data curation, formal analysis, methodology, visualization, tissue assays, and writing, including review and editing. Minjun Du was responsible for data curation, formal analysis, methodology, visualization, tissue assays, and writing, including review and editing. Yangyang Lei: Conceptualization, Formal Analysis, Investigation, Software, Writing – review & editing. Yushun Gao contributed to the conceptualization, investigation, and methodology of the project, managed the project, and participated in writing, reviewing, and editing. Shanqing Li was responsible for conceptualization, funding acquisition, investigation, methodology, project administration, resource management, supervision, and both the original draft and review/editing of the writing.

Funding

This research received funding from the China Postdoctoral Science Foundation (Grant No.2023M744038), the Guangdong Basic and Applied Research Foundation (Grant No. 2023A1515110872), the Special Research Fund for Central Universities, PekingUnion Medical college (Grant No. 3332024044&3332025012), National High Level Hospital Clinical Research Funding.

Data availability

This study utilized public data sourced from the GEO and TCGA databases.

Declarations

Ethics approval and consent to participate

Sequencing data for this study were sourced from public databases, eliminating the need for additional ethical approval. The analysis of clinical cohort data adhered to the Declaration of Helsinki. The Institutional Review Board of Cancer Hospital, Chinese Academy of Medical Sciences and Peking Union Medical College approved the study protocol, and the retrospective analysis of de-identified clinical data was exempted from requiring written informed consent.

Consent for publication

Not applicable.

Competing interests

The authors declare no competing interests.

Author details

[1]Department of Thoracic Surgery, Peking Union Medical College Hospital, Chinese Academy of Medical Sciences and Peking Union Medical College, Beijing, P. R. China
[2]Department of Thoracic Surgery, National Cancer Center/National Clinical Research Center for Cancer/Cancer Hospital, Chinese Academy of Medical Sciences and Peking Union Medical College, Chaoyang District, Panjiayuan, Nanli 17, Beijing 100021, China
[3]Department of Ultrasound, National Cancer Center/National Clinical Research Center for Cancer/Cancer Hospital, Chinese Academy of Medical Sciences and Peking Union Medical College, Beijing, China

Received: 20 December 2025 / Accepted: 7 April 2026
Published online: 17 April 2026

References

1. Deng HY, Zeng M, Li G, et al. Lung Adenocarcinoma has a Higher Risk of Lymph Node Metastasis than Squamous Cell Carcinoma: A Propensity Score-Matched Analysis. World J Surg. 2019;43(3):955–62.
2. Succony L, Rassl DM, Barker AP, McCaughan FM, Rintoul RC. Adenocarcinoma spectrum lesions of the lung: Detection, pathology and treatment strategies. Cancer Treat Rev. 2021;99:102237.
3. Xu L, Su H, She Y, et al. Which N Descriptor Is More Predictive of Prognosis in Resected Non-small Cell Lung Cancer: The Number of Involved Nodal Stations or the Location-Based Pathological N Stage? Chest. 2021;159(6):2458–69.
4. Xu L, Si H, Su H, et al. The number of metastatic lymph nodes is more predictive of prognosis than location-based N stage for nonsmall cell

lung cancer: a retrospective cohort study. Int J Surg (London England). 2023;109(12):4126–34.
5. Lee CK, Jeong SH, Jang C, et al. Tumor metastasis to lymph nodes requires YAP-dependent metabolic adaptation. Sci (New York NY). 2019;363(6427):644–9.
6. Yuan L, Jiang H, Jia Y, et al. Fatty Acid Oxidation Supports Lymph Node Metastasis of Cervical Cancer via Acetyl-CoA-Mediated Stemness. Adv Sci (Weinh). 2024;11(21):e2308422. https://doi.org/10.1002/advs.202308422.
7. Zhang C, Liao Y, Liu P, et al. FABP5 promotes lymph node metastasis in cervical cancer by reprogramming fatty acid metabolism. Theranostics. 2020;10(15):6561–80.
8. Jeon YG, Kim YY, Lee G, Kim JB. Physiological and pathological roles of lipogenesis. Nat metabolism. 2023;5(5):735–59.
9. Hoy AJ, Nagarajan SR, Butler LM. Tumour fatty acid metabolism in the context of therapy resistance and obesity. Nat Rev Cancer. 2021;21(12):753–66.
10. Santos CR, Schulze A. Lipid metabolism in cancer. FEBS J. 2012;279(15):2610–23.
11. Migita T, Narita T, Nomura K, et al. ATP citrate lyase: activation and therapeutic implications in non-small cell lung cancer. Cancer Res. 2008;68(20):8547–54.
12. Xiao J, Cao S, Wang J, et al. Leptin-mediated suppression of lipoprotein lipase cleavage enhances lipid uptake and facilitates lymph node metastasis in gastric cancer. Cancer Commun (London England). 2024;44(8):855–78.
13. Lala PK, Nandi P, Majumder M. Roles of prostaglandins in tumor-associated lymphangiogenesis with special reference to breast cancer. Cancer Metastasis Rev. 2018;37(2–3):369–84.
14. Wright HJ, Hou J, Xu B, et al. CDCP1 drives triple-negative breast cancer metastasis through reduction of lipid-droplet abundance and stimulation of fatty acid oxidation. Proc Natl Acad Sci USA. 2017;114(32):E6556–65.
15. Thorsson V, Gibbs DL, Brown SD, et al. The Immune Landscape of Cancer. Immunity. 2018;48(4):812–e830814.
16. Gong Z, Du M, Li Y, et al. Machine learning identifies TIME subtypes linking EGFR mutations and immune states in lung adenocarcinoma. NPJ Digit Med. 2025;8(1):796.
17. Xu M, Zhao X, Wen T, Qu X. Unveiling the role of KRAS in tumor immune microenvironment. Biomed pharmacotherapy = Biomedecine pharmacotherapie. 2024;171:116058.
18. Eklund EA, Svensson J, Näslund LS, et al. Comprehensive genetic variant analysis reveals combination of KRAS and LRP1B as a predictive biomarker of response to immunotherapy in patients with non-small cell lung cancer. J experimental Clin cancer research: CR. 2025;44(1):75.
19. Skoulidis F, Goldberg ME, Greenawalt DM, et al. STK11/LKB1 Mutations and PD-1 Inhibitor Resistance in KRAS-Mutant Lung Adenocarcinoma. Cancer Discov. 2018;8(7):822–35.
20. Li A, Wang Y, Yu Z, et al. STK11/LKB1-Deficient Phenotype Rather Than Mutation Diminishes Immunotherapy Efficacy and Represents STING/Type I Interferon/CD8(+) T-Cell Dysfunction in NSCLC. J Thorac oncology: official publication Int Association Study Lung Cancer. 2023;18(12):1714–30.
21. Chang TM, Chu PY, Hung WC, et al. c-Myc promotes lymphatic metastasis of pancreatic neuroendocrine tumor through VEGFC upregulation. Cancer Sci. 2021;112(1):243–53.
22. Koundouros N, Poulogiannis G. Reprogramming of fatty acid metabolism in cancer. Br J Cancer. 2020;122(1):4–22.
23. Ke X, Li K, Jiang A, Zhang Y, Wang Q, Li Z, et al. Cloud-Based GWAS Platform: An Innovative Solution for Efficient Acquisition and Analysis of Genomic Data. Med Research. 2025;1(3):397–411.
24. Zhang P, Liang X, Ye B, et al. Metabolic reprogramming signature predicts immunotherapy efficacy in lung adenocarcinoma: Targeting SLC25A1 to overcome immune resistance. Chin J cancer Res = Chung-kuo yen cheng yen chiu. 2025;37(6):1000–19.
25. Sun H, Zhang L, Wang Z, et al. Single-cell transcriptome analysis indicates fatty acid metabolism-mediated metastasis and immunosuppression in male breast cancer. Nat Commun. 2023;14(1):5590.
26. Abrego J, Sanford-Crane H, Oon C, et al. A Cancer Cell-Intrinsic GOT2-PPARδ Axis Suppresses Antitumor Immunity. Cancer Discov. 2022;12(10):2414–33.
27. Liang XH, Chen XY, Yan Y, et al. Targeting metabolism to enhance immunotherapy within tumor microenvironment. Acta Pharmacol Sin. 2024;45(10):2011–22.
28. Puente-Cobacho B, Esteo C, Altea-Manzano P, et al. De novo lipogenesis protects dormant breast cancer cells from ferroptosis and promotes metastasis. Redox Biol. 2025;80:103480.
29. Ren H, Wang M, Ma X, An L, Guo Y, Ma H. METTL3 in cancer-associated fibroblasts-derived exosomes promotes the proliferation and metastasis and suppresses ferroptosis in colorectal cancer by eliciting ACSL3 m6A modification. Biol Direct. 2024;19(1):68.
30. Xie Y, Wang B, Zhao Y, et al. Mammary adipocytes protect triple-negative breast cancer cells from ferroptosis. J Hematol Oncol. 2022;15(1):72.
31. Wu D, Wang Z, Zhang Y, et al. IL15RA-STAT3-GPX4/ACSL3 signaling leads to ferroptosis resistance in pancreatic cancer. Acta Biochim Biophys Sin. 2024;57(3):389–402.
32. Cao Y, Li J, Chen Y, et al. Monounsaturated fatty acids promote cancer radioresistance by inhibiting ferroptosis through ACSL3. Cell Death Dis. 2025;16(1):184.
33. Ubellacker JM, Tasdogan A, Ramesh V, et al. Lymph protects metastasizing melanoma cells from ferroptosis. Nature. 2020;585(7823):113–8.
34. Huang L, Xu R, Chen S, et al. Modulating lipid metabolism by nanoparticles (NPs)-mediated ACSL3 silencing to inhibit hepatocellular carcinoma growth and metastasis. Mol Cancer. 2025;24(1):73.
35. Saliakoura M, Reynoso-Moreno I, Pozzato C, et al. The ACSL3-LPIAT1 signaling drives prostaglandin synthesis in non-small cell lung cancer. Oncogene. 2020;39(14):2948–60.
36. Rossi Sebastiano M, Pozzato C, Saliakoura M, Yang Z, Peng RW, Galiè M, et al. ACSL3-PAI-1 signaling axis mediates tumor-stroma cross-talk promoting pancreatic cancer progression. Sci Adv. 2020;6(44):eabb9200.
37. Fernández LP, Merino M, Colmenarejo G, et al. Metabolic enzyme ACSL3 is a prognostic biomarker and correlates with anticancer effectiveness of statins in non-small cell lung cancer. Mol Oncol. 2020;14(12):3135–52.
38. He T, Hu J, Guo H, et al. Lipid Metabolism Related Gene ACSL3 as a Biomarker for Predicting Immunotherapy Outcomes in Lung Adenocarcinoma. Cancer Res Treat. 2025;57(4):1000–18.
39. Chen J, Ding C, Chen Y, et al. ACSL4 promotes hepatocellular carcinoma progression via c-Myc stability mediated by ERK/FBW7/c-Myc axis. Oncogenesis. 2020;9(4):42.
40. Chen J, Ding C, Chen Y, et al. ACSL4 reprograms fatty acid metabolism in hepatocellular carcinoma via c-Myc/SREBP1 pathway. Cancer Lett. 2021;502:154–65.
41. Jia Y, Yan Q, Zheng Y, et al. Long non-coding RNA NEAT1 mediated RPRD1B stability facilitates fatty acid metabolism and lymph node metastasis via c-Jun/c-Fos/SREBP1 axis in gastric cancer. J experimental Clin cancer research: CR. 2022;41(1):287.
42. Pascual G, Avgustinova A, Mejetta S, et al. Targeting metastasis-initiating cells through the fatty acid receptor CD36. Nature. 2017;541(7635):41–5.
43. Li Z, Kang Y. Lipid Metabolism Fuels Cancer's Spread. Cell Metabol. 2017;25(2):228–30.
44. Shang C, Wang W, Liao Y, et al. LNMICC Promotes Nodal Metastasis of Cervical Cancer by Reprogramming Fatty Acid Metabolism. Cancer Res. 2018;78(4):877–90.
45. Shang C, Li Y, He T, et al. The prognostic miR-532-5p-correlated ceRNA-mediated lipid droplet accumulation drives nodal metastasis of cervical cancer. J Adv Res. 2022;37:169–84.
46. Zhong S, Guo Q, Chen X, et al. The inhibition of YTHDF3/m(6)A/LRP6 reprograms fatty acid metabolism and suppresses lymph node metastasis in cervical cancer. Int J Biol Sci. 2024;20(3):916–36.
47. Wang Y, Hu M, Cao J, et al. ACSL4 and polyunsaturated lipids support metastatic extravasation and colonization. Cell. 2025;188(2):412–e429427.
48. Zhang X, Hu X, Fu C, et al. Novel MAFG-METTL14-SCD1 axis regulates lipid metabolism mediating choroidal melanoma distant metastasis. J experimental Clin cancer research: CR. 2025;44(1):334.
49. Mao X, Lei H, Yi T, et al. Lipid reprogramming induced by the TFEB-ERRα axis enhanced membrane fluidity to promote EC progression. J experimental Clin cancer research: CR. 2022;41(1):28.
50. Peng S, Li Y, Huang M, et al. Metabolomics reveals that CAF-derived lipids promote colorectal cancer peritoneal metastasis by enhancing membrane fluidity. Int J Biol Sci. 2022;18(5):1912–32.
51. Liu C, Li M, Dong ZX, et al. Heterogeneous microenvironmental stiffness regulates pro-metastatic functions of breast cancer cells. Acta Biomater. 2021;131:326–40.
52. Zheng Y, Zhou R, Cai J, et al. Matrix Stiffness Triggers Lipid Metabolic Crosstalk between Tumor and Stromal Cells to Mediate Bevacizumab Resistance in Colorectal Cancer Liver Metastases. Cancer Res. 2023;83(21):3577–92.

Publisher's note